# Effect of Component Geometry on Flow Nonuniformities in a Large Pulse Tube Cryocooler

**M. A. Lewis[1], R. P. Taylor[1,2], R. Radebaugh[1], and P. E. Bradley[1]**

[1]National Institute of Standards and Technology. Boulder, CO 80305
[2]Virginia Military Institute, Lexington, VA 24450

## ABSTRACT

A single-stage pulse tube cryocooler was designed to achieve 50 W of refrigeration power at 50 K when driven by a pressure oscillator that can produce up to 2.8 kW of acoustic power at 60 Hz. Initial experimental data produced no-load temperatures that were considerably higher than expected. Improvements were made to the warm end heat exchanger, aftercooler, and diffusion-bonding of the copper screen matrix materials, which produce significant improvements to the low-end temperatures. The primary diagnostic tools utilized were four equidistant azimuthally spaced thermocouples located at the aftercooler exit and at the center planes of the regenerator component and the pulse tube component. The tools provided the information on the temperature distribution throughout the system and how the specific geometry changes throughout the pulse tube cryocooler would affect overall performance. This paper addresses the specific geometry changes to several major components of the cryocooler and their effect on the cryocooler performance. These include the transition piece from the inertance tube where the helium gas is entering and exiting the warm end heat exchanger and the pulse tube. Pulse tubes with various aspect ratios are tested to find the optimum aspect ratio. A major modification to the cold end heat exchanger matrix design will be implemented for more uniform gas flow through the diffusion bonded copper screen stacks. The effect of interspersing various amounts of copper screen along the stainless steel regenerator packing is also investigated.

## INTRODUCTION

The purpose of the described pulse tube cryocooler is to provide cooling for a high-temperature superconducting (HTS) magnet made from a second-generation Yttrium Barium Copper Oxide (YBCO) wire that is part of a gyrotron. The specific application of this cryocooler is to provide cooling for the HTS magnet for tactical deployment of an Active Denial System (ADS) that utilizes high-power (5 MW) mm-wave (95 GHz) beams. The baseline optimized pulse tube cryocooler was designed to provide a minimum of 50 W of net refrigeration power at 50 K by use of a commercial, dual opposed-piston, pressure-wave generator. The rated performance of the pressure-wave generator is 2.0 kW of delivered acoustic power under correct impedance-matching at a nominal driving frequency of 60 Hz. This system also incorporates a previously developed fast cool-down technique that makes use of a resonance phenomenon in the inertance tube and reservoir system to

*Cryocoolers 16,* edited by S.D. Miller and R.G. Ross, Jr.

decrease the flow impedance and thereby increase the acoustic power flow through the system by about a factor of four above the optimized steady-state value used when the cold tip is at 50 K.[1,2,3,4,5] The reduced flow impedance obtained with the resonance phenomenon also provides a better impedance match to the pressure oscillator when the cold end is warm, which results in higher compressor system efficiency during the initial cool-down period, in addition to, that of the target cooling temperature. A schematic of the developed pulse tube cryocooler is illustrated in Figure 1.

Previously reported work on the development and implementation of the aforementioned pulse tube cryocooler indicated severe flow mal-distribution losses present in the regenerator matrix as well as in the pulse tube component.[6,7] The results of this prior work identified three areas of the system that were the likely sources of significant flow mal-distribution losses: 1) the pulse tube component, 2) the cold and 3) and warm end pulse tube heat exchangers, as the likely culprit due to the presence of severe thermal gradients in the azimuthal plane at the center point of the pulse tube component. However, competing effects due to the hydraulic resistance of the heat exchange matrices at either end of the pulse tube component were also recognized as potential sources of flow mal-distribution either inducing or amplifying the severe thermal gradients documented in the pulse tube component. The construction of these heat exchange matrices involved the uses of pie-shaped, diffusion-bonded, copper wire mesh screen. This particular arrangement was developed to enhance the radial thermal conductance of the heat exchange matrices due to the large radial-to-axial aspect ratio, which leads to poor radial thermal conductance for a solid wire mesh screen pack. Initial tests indicated that use of the pie shaped segments led to nonuniform hydraulic resistance in the various quadrants. This effect was theorized to significantly affect the hydrodynamic performance via the addition of complex mixing effects and jetting in the pulse tube component. Furthermore, while each heat exchanger utilizes the pie-shaped heat exchange designs, the hot heat exchanger was identified as the primary source of any induced hydrodynamic instability. This is primarily attributed to the fact that the gas exiting the inertance tube is at a high velocity, and must rapidly equilibrate to the larger cross section. This paper reports on the development of alternative designs for the pulse tube cryocooler to mitigate the flow mal-distribution losses. The specific areas investigated were the pulse tube aspect ratio, the warm-end heat exchanger and flow transition configuration, and the cold-end heat exchanger configuration. Experimental results and future areas of improvement are discussed.

## EXPERIMENTAL DESIGN PERMUTATIONS

To isolate and ultimately correct the poor performance for the developed pulse tube cryocooler, various geometric permutations were incorporated to arrive at a system configuration capable of

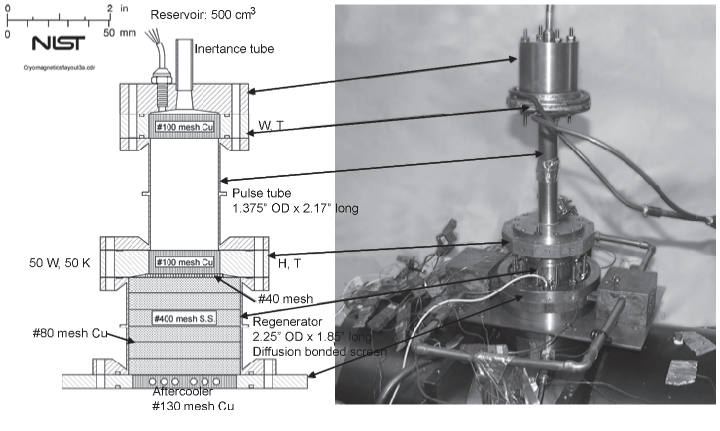


**Figure 1**. Schematic of the rapid cooldown pulse tube cooler with photograph illustrating the manufactured components.

achieving the target refrigeration load. The specific changes incorporated into the pulse tube cryocooler design included:

1. the pulse tube aspect ratio,
2. the warm-end heat exchanger configuration to include the flow transitioning from the pulse tube to the warm heat exchanger, and
3. the cold-end heat exchange matrix configuration.

These specific areas are addressed in detail in the following subsections.

**Pulse Tube Aspect Ratio**

One of the critical areas associated with performance of a pulse tube cryocooler is the pulse tube component itself. In the case of the pulse tube component, the sole purpose is to provide highly ordered, thermally stratified flow to facilitate efficient enthalpy transport up a temperature gradient. Often empirical rules of thumb are utilized to design this component. More specifically, the design rule of thumb involves sizing the pulse tube component such that the volume is approximately 3 to 5 times the cold end swept gas volume. This should allow sufficient gas expansion space while limiting the linear displacement of the gas in the pulse tube component. While this rule of thumb does yield a valid specification for the pulse tube gas volume, the geometric aspect ratio of the pulse tube is typically arrived at via costly experimental permutations to yield optimum system performance. However, recent work by Taylor et al.[8,9] has utilized a two-dimensional axisymmetric computational fluid dynamic model of the pulse tube component to determine the optimum pulse tube aspect ratio in terms of a pulse tube figure of merit (FOM) defined as:

$$FOM = \frac{\left\langle \dot{H}_{PT} \right\rangle}{\left\langle P\dot{V}_{PT} \right\rangle} \tag{1}$$

where $\langle \dot{H}_{PT} \rangle$ is the time-averaged enthalpy flow in the pulse tube and $\langle P\dot{V}_{PT} \rangle$ is the time-averaged acoustic power flow in the pulse tube component. In the work by Taylor et al.[8,9] the choice of the pulse tube aspect ratio differs relative to that of other researchers in that the aspect ratio is defined as a dimensionless scaling parameter relative to the fixed diameter of the regenerator and inertance tube. The chosen pulse tube aspect ratio, also referred to as the dimensionless pulse tube diameter, is expressed as,

$$\bar{D}_{PT} = \frac{D_{PT} - D_{IN}}{D_{REG} - D_{IN}} \tag{2}$$

where $D_{PT}$ is the diameter of the pulse tube, $D_{REG}$ is the diameter of the regenerator, and $D_{IN}$ is the diameter of the inertance tube. The results of this work showed that there exists an optimum dimensionless pulse tube diameter at which the conversion of acoustic power flow to enthalpy flow in the pulse tube is maximized. A characteristic plot of this relationship is illustrated in Figure 2 for a large capacity pulse tube cryocooler similar to the one discussed herein. Observation of the results in Figure 2 show that the optimum pulse tube aspect ratio occurs at relatively low values of the dimensionless pulse tube diameter. These results indicate that the ideal pulse tube is long and slender (i.e., more closely matches the diameter of the inertance tube). However, the results indicate that a pulse tube that is excessively long and slender hinders performance as the boundary layer heat flux becomes sizable due to the diameter of the pulse tube approaching the thickness of the thermal boundary layer.

In the original pulse tube configuration, the dimensionless pulse tube diameter was determined to be 0.55. Based upon the results of the CFD modeling predictions by Taylor[8,9] this value is relatively high compared to the predicted optimum value. In an effort to increase the conversion of acoustic power to enthalpy flow, two new pulse tube designs were developed that more closely follow the trends indicated in Figure 2. The geometric dimensions of the original and new pulse tube designs are summarized in Table 1, and the physical size of the three pulse tube permutations are shown in Figure 3.

Note that while the above figure illustrated that the ideal non-dimensional pulse tube diameter occurs at ~0.2, the new pulse tube designs have higher values for the dimensionless diameter. These

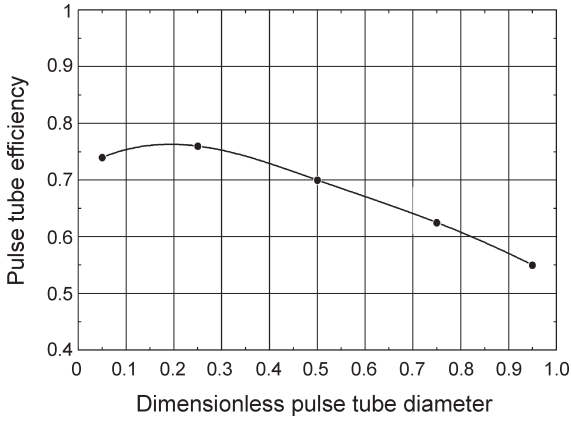


**Figure 2**. Plot illustrating a representative curve for the figure of merit (FOM) of a pulse tube component as a function of a dimensionless pulse tube diameter.

**Table 1:** Experimental pulse tube geometry

| Parameter | Short Pulse Tube | Medium Pulse Tube | Long Pulse Tube |
|---|---|---|---|
| Inside diameter (mm) | 33.53 | 24.56 | 21.69 |
| Length (mm) | 55.27 | 104.78 | 133.35 |
| Dimensionless diameter | 0.55 | 0.37 | 0.31 |

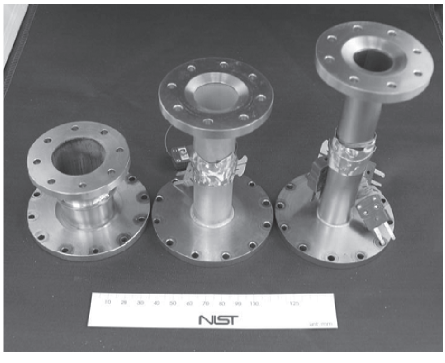

**Figure 3**. Photo illustrating the constructed pulse tube permutations with aspect ratios of 0.31, 0.37, and 0.55.

values were chosen due to structural and packaging constraints. As the pulse tube length is increased, the stresses in the pulse tube component increase due to the size of the hot heat exchanger and inertance tube transition. Additionally, lengthening the pulse tube substantially increases the physical size of the system, which is currently limited by the vacuum chamber in use.

### Cold Heat Exchanger Configuration

Due to the physical size of the regenerator component and the anticipated heat loads at the cold heat exchanger, efficient radial conductance was desired. As a result, the original cold heat exchanger design was manufactured such that the heat exchange matrix was divided into quadrants with solid sections of copper separating each. This was done to aid in the thermal radial conductance between the applied heat load and the internal gas flow. Previous work by Lewis et al.[6] identified this configuration as problematic from the standpoint of hydrodynamic instability driven by the quadrant configuration. More specifically, while the quadrant configuration is superior from

a strictly heat-transfer viewpoint, hydrodynamic instability is inherent in this configuration. The hydrodynamic instability is driven solely by the variable hydrodynamic resistance present in the screen stacks. While the screen quadrants were manufactured from a single monolithic block of diffusion-bonded screens, there exist variance in the porosity and hydrodynamic resistance due to manufacturing, nonuniform loading during the diffusion bonding process, and human error in arranging the screens prior to diffusion bonding. In an effort to mitigate flow mal-distribution due to the hydrodynamic resistance of the heat exchanger, a new set of copper screens was diffusion bonded while improving control of the order of the screens as well as the loading of the screens during the diffusion-bonding process. Additionally, the quadrant design was eliminated, and instead a solid core heat exchange matrix was machined and diffusion-bonded into a new heat exchanger flange. Note that the size of the heat exchange flange was identical to the pie-shaped flange, with the only difference being the elimination of the quadrant configuration. The two cold heat exchanger permutations are shown in Figure 4.

**Warm Heat Exchanger Configuration**

The original configuration of the warm heat exchanger for the pulse tube cryocooler was designed in a fashion similar to that of the cold end heat exchanger. The heat exchange matrix was divided into quadrants, with a solid copper section separating each quadrant to aid in radial thermal conductance. Lewis et al.[6] described numerous problems with this configuration related to the thermal stratification in the pulse tube component. More specifically, it was found that the hydrodynamic instability introduced by the quadrant configuration at the warm end heat exchanger had a more significant impact on system performance than at the cold end heat exchanger. Due to the relatively large mass flow rates present in the designed cryocooler, the velocity of the gas exiting the inertance tube is substantially higher than the bulk gas flow in the pulse tube component. Consequently, this high velocity gas flow must be rapidly decelerated before entering the heat exchanger matrix while allowing for sufficient radial equilibration. In the quadrant configuration, if any of the sectors are of different hydrodynamic resistance than the rest, the high velocity gas will take the path of least resistance through the heat exchange matrix.

This is detrimental, as the effective diameter of the heat exchanger is reduced, because the flow is preferential to a single quadrant. This reduces the heat rejection, leading to higher average gas temperatures entering the pulse tube. Furthermore, the gas flow passing through the wire mesh screen does not radially equilibrate due to the anisotropic flow resistance inherent in packed wire mesh screen. The net effect of these two items is that a high velocity jet of hot gas enters the pulse tube which subsequently destroys the thermal stratification in the pulse tube. This effect was visualized and documented by Garaway et al.[7] and isolated experimentally via addition of a rudimentary flow straightener, as discussed by Lewis et al.[6]

In an effort to mitigate this jetting effect and subsequent performance penalty, the warm end heat exchanger was redesigned such that the diameter of the warm end heat exchanger matched the diameter of the pulse tube with a non-dimensional diameter of 0.31. The heat exchange matrix was

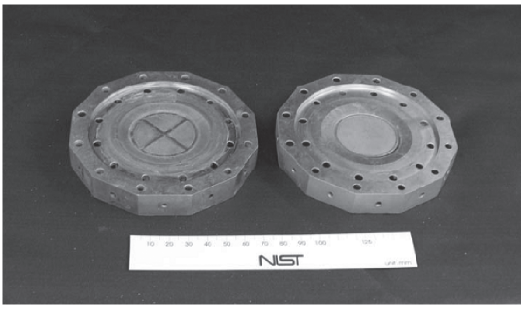


**Figure 4**. Photograph illustrating the cold end heat exchanger for (left) a pie-shaped heat exchange configuration to maximize radial conductance, and (right), a solid-core diffusion-bonded screen stack.

fashioned from diffusion-bonded copper #60 wire mesh screen. The heat exchanger was matched to the large aspect ratio of the pulse tube, as the experimental measurements, showed this design to be superior to the other two pulse tube designs. Additionally, to aid in radial equilibration and deceleration of the flow exiting the inertance tube, the flow was transitioned in a conical tapered section before it entered the warm end heat exchanger. The taper angle was set at 8 degrees from the centerline, with a linear distance of about 1 inch.

## EXPERIMENTAL METHODOLOGY

To evaluate the system-level performance of the developed pulse tube cryocooler as a function of permutations in pulse tube aspect ratio, cold heat exchanger design, and warm heat exchanger design, diagnostic temperature measurements were performed. To evaluate the overall system performance, the no-load cold-end temperature was measured with two NTC RTD temperature sensors attached to the cold-end heat exchanger spaced 180 degrees apart. To evaluate the performance of the warm-end heat exchanger, the inlet and outlet water temperatures were measured with calibrated type T thermocouples, and the water volume flow rate was measured with a commercial rotameter. The effect of the various geometric permutations on the flow profile in the pulse tube component and the regenerator component were quantified via measurements of four equidistant azimuthally spaced type T calibrated thermocouples located at the axial center location of the pulse tube and regenerator tube walls. To determine the pressure amplitudes present in the experimental system, required for computation of the phase angles and the acoustic power flow, piezo-resistive and piezoelectric pressure transducers were used that were located at the warm end heat exchanger and the reservoir volume. From the measurement of the pressure signals, the phase angles were determined by utilizing commercial DSP lock-in amplifiers in which all signals were referenced to the reservoir pressure signal.

## EXPERIMENTAL RESULTS

The initial experimental results for the prototype cooler yielded a low-end temperature of about 102 K, as discussed by Lewis et al.[2,6] but showed severe azimuthal temperature gradients in the pulse tube and regenerator components; see Table 2. The design models predicted much lower temperatures, which indicate significant losses in the cryocooler. The initial tests used the original cryocooler design, which consisted of the small aspect ratio pulse tube and the pie-shaped cold and warm-end heat exchangers. Based upon the poor initial performance of the designed pulse tube cryocooler, initial efforts described by Lewis et al.[2,6] focused on fixing clear sources of system losses, such as the aftercooler and use of a rudimentary flow transition in the pulse tube component to identify whether flow mal-distribution was a dominant loss. Flow mal-distribution was suspected due to the high pulse tube temperature as well as the presence of large azimuthal temperature gradients in the pulse tube component. Replacement of the aftercooler with a new design yielded higher compressor heat rejection and a subsequent lower inlet temperature to the regenerator. The new aftercooler design yielded better performance with a no-load cold end temperature of 85 K. This change in geometry resulted in lower temperature in both the regenerator and the pulse tube, in addition to a more uniform temperature distribution around the center-line; see Table 2. To determine the severity of flow mal-distribution in the pulse tube component, a rudimentary flow straightener in the warm end of the pulse tube was used. This flow straightener consisted of two layers of

**Table 2:** Initial experimental results.

| Configuration | No-Load Temp (K) | Regenerator Temps (K) | Pulse Tube Temps (K) |
|---|---|---|---|
| Original Design | 102 | 214 196<br>205 203 | 221 260<br>261 237 |
| New Aftercooler | 85 | 197 179<br>203 207 | 192 164<br>193 198 |
| Aftercooler w/Simple Flow Transition | 65 | 192 161<br>193 198 | 123 130<br>129 130 |

#40 mesh copper backed with a diffusion-bonded screen stack consisting of two #400 mesh stainless steel screen and a single #24 mesh stainless steel screen. Using the flow transition in conjunction with the new aftercooler, a no-load low-end temperature of 65 K was achieved. This result indicated the presence of severe flow mal-distribution. In addition to the lower no-load temperature, the azimuthal temperature gradient around the center line for both the regenerator and pulse tube were significantly improved. The initial experimental results are summarized in Table 2.

Based upon this initial work, the next logical task was to utilize the previously mentioned alternate designs for the pulse tube aspect ratio, the warm end heat exchanger configuration, and the cold end heat exchanger configuration to determine the effects on the system performance. The results from these measurements are elaborated in more detail in the following subsections.

**Effect of Pulse Tube Aspect Ratio**

Based upon the results presented in Figure 2 from work by Taylor et al.,[8,9] increasing the aspect ratio (lowering the dimensionless diameter) should increase system performance via a higher FOM for the pulse tube component. Furthermore, lengthening of the pulse tube typically improves thermal stratification and aids in higher enthalpy transport up the temperature gradient. An additional benefit to this is that the axial conduction loss is reduced, aiding in useful cooling. The initial experimental measurement consisted of replacing the original short pulse tube with the new medium and long pulse tube designs; the dimensions of the pulse tubes are summarized in Table 1. Operation of the pulse tube cryocooler with the medium aspect ratio pulse tube yielded a no-load low-end temperature of 47.5 K. This temperature represents a rather large improvement in system performance, which was predicted by the CFD model. Observation of the temperature distribution around both the regenerator and pulse tube indicated that the previously witnessed large azimuthal temperature gradients were close in temperature values, although the pulse tube temperature was significantly higher than design predictions. Installation of the large aspect ratio pulse tube resulted in a no-load low-end temperature of 44 K. This pulse tube produced improved uniformity in the temperature distribution around both the regenerator and the pulse tube components. The pulse tube temperature remained much higher than the model predictions. Operation of the pulse tube cryocooler with the large aspect ratio pulse tube yielded a no-load low-end temperature of 42.9 K. This result, much like the medium aspect ratio pulse tube, represents a large improvement in system performance, as predicted by the CFD model. As with the medium aspect ratio pulse tube, the large aspect ratio had minimal azimuthal temperature gradients in the pulse tube and the regenerator. However, one of the problem areas identified with each of the new pulse tube configurations was the rather large temperature at the center section of the pulse tube component, as shown in the Table 3. The results of these measurements are summarized in Tables 2 and 3.

Additional quantification of the performance impact of the new pulse tube designs involved determining the FOM for each of the pulse tubes components tested. Utilizing the measurement of the no-load temperature in addition to the computed heat rejection at the warm heat exchanger and the PV power flow at the warm end, the FOM for each of the test experimental pulse tubes was computed. The results of this analysis are presented in Table 2.

As the results in Table 3 show, increasing the aspect ratio of the pulse tube component strongly effected the performance of the pulse tube cryocooler. As the aspect ratio was increased, the resulting no-load temperature, and by extension the cooling power, were sizably increased. Furthermore, the addition of the matched diameter heat exchanger and the conical warm end flow transition

**Table 3:** Comparison of pulse tube performance

| Configuration | Temperature (K) | $Q_{HHX}$ (W) | PV Power (W) | FOM |
|---|---|---|---|---|
| Original Aspect Ratio PT | 85 | 110.3 | 203 | 0.54 |
| Medium Aspect Ratio PT | 47.5 | 118.2 | 150.2 | 0.78 |
| Large Aspect Ratio PT | 44 | 118.2 | 127.9 | 0.92 |
| Large Aspect Ratio PT w/new hot heat exchanger | 42.9 | 118.2 | 120 | 0.985 |

enabled the FOM for the pulse tube component to approach the ideal value of unity. The results of this analysis clearly show that the pulse tube aspect ratio and the warm end heat exchanger configuration play critical roles in the performance of the overall system.

**Effect of Cold End Heat Exchanger Configuration**

To investigate the effects of the pie-segmented cold-end heat exchanger, the original heat exchanger design was replaced with a heat exchanger of similar geometry in which the pie segments were replaced with a single solid #100 mesh copper diffusion-bonded screen stack. The large aspect ratio pulse tube was used with this cold-end heat exchanger, as it provided the best case no-load temperature. The experimental data resulted in a no-load low-end temperature of 50.8 K with an approximately identical regenerator and pulse tube temperature distribution observed with the pie-segmented cold-end heat exchanger. This temperature compares poorly to the previously measured no-load temperature of 44 K with the pie-shaped heat exchanger. The results of this analysis indicate that the cold heat exchanger is functioning correctly. The results from this set of measurements are summarized in Table 4.

**Effect of Warm End Heat Exchanger Configuration**

To improve the temperature performance within the pulse tube, the warm-end heat exchanger and the inertance tube flange were replaced with geometry compatible to smaller diameter pulse tube dimensions as seen in Figure 5. These high temperatures indicate that the warm-end heat exchanger is not adequate to reject the amount of heat required for pulse tube efficiency. The new warm-end heat exchanger was modified to a length of 19.05 mm. The inside diameter was 21.6 mm, which matched the geometry of the pulse tube of large aspect ratio. The matrix of the heat exchanger was #60 mesh diffusion-bonded copper screen. The inertance tube flange was fashioned for a uniform flow transition from the inertance tube into the warm-end heat exchanger, utilizing approximately a 9 degree taper from the exit of the inertance tube into the heat exchanger. The length of the transition flange was 50.8 mm. The geometry that produced the best no-load temperature of 44 K was used to evaluate the performance of the new warm-end heat exchanger and new inertance tube flange. The experimental results produced a no-load low-end temperature of 42.9 K.

**Table 4:** Experimental results using new pulse tubes and cold-end heat exchanger

| Test Configuration | No-Load Temp (K) | Regenerator Temps (K) | Pulse Tube Temps (K) |
|---|---|---|---|
| Large Aspect Ratio PT<br>Cold HX Quadrants | 44 | 177 161<br>174 176 | 258 262<br>260 259 |
| Large Aspect Ratio PT<br>Cold HX Disk | 50.8 | 170 153<br>176 177 | 255 263<br>266 265 |

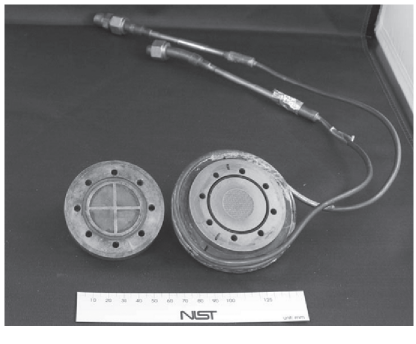


**Figure 5**. Photograph illustrating the warm end heat exchanger using (left) a quadrant configuration, and (right) using a solid screen stack in which the heat exchanger diameter is matched to the pulse tube diameter.

Temperatures in the pulse tube component were lowered by about 51 K and remained uniform around the pulse tube circumference. The temperatures of the regenerator component remained about the same. The mass flow achieved at the warm-end was about 7.6 g/s and the design model predictions are about 30 % higher. In order to achieve the required mass flow rate, design modification to the inertance tube will need to be evaluated. Initial efforts to quantify this approach were performed via shortening the original inertance tube by 549 mm to change the impedance and observe the effects. This resulted in a no-load low-end temperature of 41.3 K. There were no improvements to the mass flow rate, but this change lowered the phase angle at the warm-end which provided additional cooling of 1.6 K. The temperature in both the regenerator and pulse tube component were lowered by about 9 K and 25 K, respectively. The results for these experiments are tabulated in Table 4. Heat-load experiments were performed on the low-end temperatures achieved at 42.9 K and 41.3 K, which indicated a net refrigeration power of 17.7 W and 20.5 W, respectively.

## CONCLUSIONS

This paper has presented the design of a pulse tube cryocooler of large capacity. Initial experiments indicated the presence of large parasitic heat loads that severely degraded the expected performance. Large pulse tube cryocoolers are susceptible to flow nonuniformities in the pulse tube component, which often lead to poor performance; this effect was seen as a result of the original pulse tube cryocooler design. Various changes in the geometry of the original design were implemented to improve the overall performance. Computational fluid dynamic modeling of the pulse tube flow and the effect of the warm-end flow transition were utilized to provide guidance on how to reduce the previously documented flow mal-distribution losses. The experimental results that were achieved confirm the predictions of the CFD modeling. More specifically, the CFD model results predicted that the performance of the system should increase considerably as the aspect ratio of the pulse tube component was increased; this trend was confirmed experimentally. The primary changes in geometry that were implemented to improve the cryocooler performance were pulse tubes of higher aspect ratio, modified cold heat exchanger design, and a modified configuration of the warm end heat exchanger. Of these changes, the modification of the warm heat exchanger configuration and the larger pulse tube aspect ratio provided the largest reduction in system losses. These two changes improved the no-load low-end temperatures from 65 K to 41 K and enabled the cryocooler to achieve a net refrigeration power of about 21 W at 50 K. Further modifications are planned to improve the inertance tube to increase the flow rate about 30 % to be consistent with design values. This will provide a better impedance match to the compressor and allow for a higher mass flow rate, leading to higher acoustic power flows. A higher acoustic power flow coupled with better impedance matching should allow the designed system to provide 50 W of refrigeration at 50 K.

## ACKNOWLEDGMENT

Funding from Cryomagnetics and the U.S. Air Force is acknowledged. Additionally the authors do so thank Mike Rybowiak and Robert Gomez for careful machining of parts utilized.

## REFERENCES

1. Radebaugh, R., O'Gallagher, A., Lewis, M.A., and Bradley, P.E., Proposed Rapid Cooldown Technique for Pulse Tube Cryocoolers," *Cryocoolers 14*, ICC Press, Boulder, CO (2007), pp.231-240.
2. Lewis, M.A., Taylor, R.T., Bradley, P.E., Garaway, I., and Radebaugh, R., "Pulse Tube Cryocooler for Rapid Cooldown of a Superconducting Magnet," *Cryocoolers 15*, ICC Press, Boulder, CO (2009), pp.167-176.
3. Radebaugh, R., Lewis, M., Luo, E., Pfotenhauer, J.M., Nellis, G.F., and Schunk, L.A.,"Inertance Tube Optimization for the Pulse Tube Refrigerators," *Adv. in Cryogenic Engineering*, Vol. 51, Amer. Institute of Physics, Melville, NY (2006), pp.59-67.
4. Lewis, M.A., Bradley, P.E., Radebaugh, R., "Impedance of Inertance Tubes," *Adv. in Cryogenic Engineering*, Vol. 51, Amer. Institute of Physics, Melville, NY (2006), pp.1557-1563.

5. Luo, E., Radebaugh, R. and Lewis, M., "Inertance Tube Models and their Experimental Verification," *Adv. in Cryogenic Engineering*, Vol. 49B, Amer. Institute of Physics, Melville, NY (2004), pp.1485-1489.

6. Lewis, M.A., Taylor, R.T., Radebaugh, R. Garaway, I., and Bradley, P. E., "Investigation of Flow Nonuniformities in a Large 50 K Pulse Tube Cryocooler," *Adv. in Cryogenic Engineering*, Vol. 55, Amer. Institute of Physics, Melville, NY (2010), pp. 68-75.

7. Garaway, I., Taylor, R.T., Lewis, M.A., Bradley, P.E., and Radebaugh, R., "Characterizing Flow and Temperature Instabilities within Pulse Tube Cryocoolers Using Infrared Imaging," *Cryocoolers 15*, ICC Press, Boulder, CO (2009), pp.233-240.

8. Taylor, R.P., Nellis, G.F., and Klein, S.A., "Optimal Pulse-tube Design using Computational Fluid Dynamics," *Adv. in Cryogenic Engineering*, Vol. 53, Amer. Institute of Physics, Melville, NY (2008), pp.1401-1410.

9. Taylor, R. P., "Optimal Pulse-Tube Design using Computational Fluid Dynamics," *Ph.D. Dissertation*, University of Wisconsin-Madison, 2009.